JCI insight

RESEARCH ARTICLE

Gut microbiota–dependent modulation of innate immunity and lymph node remodeling affects cardiac allograft outcomes

Jonathan S. Bromberg,[1] Lauren Hittle,[2] Yanbao Xiong,[1] Vikas Saxena,[1] Eoghan M. Smyth,[2] Lushen Li,[1] Tianshu Zhang,[3] Chelsea Wagner,[1] W. Florian Fricke,[4] Thomas Simon,[5] Colin C. Brinkman,[1] and Emmanuel F. Mongodin[2]

[1]University of Maryland School of Medicine, Center for Vascular and Inflammatory Diseases, Departments of Surgery, Microbiology and Immunology, Baltimore, Maryland, USA. [2]University of Maryland School of Medicine, Institute for Genome Sciences, Baltimore, Maryland, USA. [3]University of Maryland School of Medicine, Department of Surgery, Baltimore, Maryland, USA. [4] Institute of Biological Chemistry and Nutrition, University of Hohenheim, Stuttgart, Germany. [5]CNRS, Institut de Pharmacologie Moléculaire et Cellulaire, Université Côte d'Azur, Valbonne, France.

We hypothesized that the gut microbiota influences survival of murine cardiac allografts through modulation of immunity. Antibiotic pretreated mice received vascularized cardiac allografts and fecal microbiota transfer (FMT), along with tacrolimus immunosuppression. FMT source samples were from normal, pregnant (immune suppressed), or spontaneously colitic (inflammation) mice. *Bifidobacterium pseudolongum* (*B. pseudolongum*) in pregnant FMT recipients was associated with prolonged allograft survival and lower inflammation and fibrosis, while normal or colitic FMT resulted in inferior survival and worse histology. Transfer of *B. pseudolongum* alone resulted in reduced inflammation and fibrosis. Stimulation of DC and macrophage lines with *B. pseudolongum* induced the antiinflammatory cytokine IL-10 and homeostatic chemokine CCL19 but induced lesser amounts of the proinflammatory cytokines TNFα and IL-6. In contrast, LPS and *Desulfovibrio desulfuricans* (*D. desulfuricans*), more abundant in colitic FMT, induced a more inflammatory cytokine response. Analysis of mesenteric and peripheral lymph node structure showed that *B. pseudolongum* gavage resulted in a higher laminin α4/α5 ratio in the lymph node cortical ridge, indicative of a suppressive environment, while *D. desulfuricans* resulted in a lower laminin α4/α5 ratio, supportive of inflammation. Discrete gut bacterial species alter immunity and may predict graft outcomes through stimulation of myeloid cells and shifts in lymph node structure and permissiveness.

Introduction

Transplantation is a routine intervention for treatment of organ failure. Renal transplantation is the most common, with success rates routinely exceeding 90%–98% after 1 year. Many variables determine outcomes, such as quality of the donor organ (e.g., living vs. deceased, older vs. younger) and recipient comorbidities (e.g., age, obesity, other organ system dysfunction). Despite major improvements in donor organ preservation, recipient selection, immunosuppressive regimens and monitoring, infection prophylaxis, and classification of rejection types, the majority of renal allografts eventually succumb to the inexorable process of organ inflammation and scarring, termed interstitial fibrosis/tubular atrophy (IF/TA) (1–3). A similar process is indicative of all transplanted organs. Thus, the rate of decline of renal function has not changed in 20 years (4). The pathophysiology of IF/TA is poorly understood, and precise diagnostic tools to predict this entity are lacking. Investigations have been dominated by analysis of adaptive immunity to alloantigens; however, IF/TA is only loosely associated with ongoing or enhanced T and B cell immunity (2, 3, 5). Indeed, the expectation has been that, since drugs and monitoring for preventing, diagnosing, and treating rejection and alloreactivity have improved, the incidence and progression of IF/TA should have decreased, although this has not occurred. While alloreactivity may be a common

Conflict of interest: The authors have declared that no conflict of interest exists.

License: Copyright 2018, American Society for Clinical Investigation.

Submitted: March 13, 2018
Accepted: August 21, 2018
Published: October 4, 2018

Reference information:
JCI Insight. 2018;3(19):e121045.
https://doi.org/10.1172/jci.insight.121045.

pathway for IF/TA, it may not be the only major upstream mechanism driving inflammation, immunity, and organ damage (2, 3, 5). Since multiple competing hypotheses have not successfully explained or intervened in IF/TA, a new approach is required.

Numerous studies linking the microbiota to inflammation strongly suggest that the microbiota is a driving force in immune dysfunction and, thus, a potential therapeutic target. The systemic inflammatory effects of the microbiota have been well documented and shown to be critical in various human conditions (6–8). However, since most studies have been associative, the specific pathways by which the microbiota interacts with the immune system remain elusive. Components of the microbiota, such as cell walls, metabolites, and nucleic acids, interact with innate and adaptive immunity through receptors on endothelial cells, innate lymphoid cells (ILC), DC, other myeloid cells, and lymphocytes (9–11). Tregs modulate the immune system, maintain tolerance to self-antigens, abrogate autoimmune disease, and may improve organ transplantion outcome. Tregs regulate the composition of the microbiota and directly recognize microbiota antigens through their antigen-specific receptors (12), while microbiota directly instruct Foxp3$^+$ Tregs (13, 14). Together, these reports demonstrate that the microbiota can trigger pro- or antiinflammatory effects that regulate local intestinal and systemic immune homeostasis (15). In the context of organ transplantation, the microbiota influence allograft rejection and graft-versus-host disease (GVHD) (16–18). However, the precise nature of the influence the microbiota exerts on alloimmunity is mostly unknown. Since the immune system and the microbiota have bidirectional interactions, the immune system is altered by immunosuppression, and the antibiotics administered to allograft recipients alter the microbiota (19, 20), these findings provide the rationale for characterizing the microbiota of allograft recipients and determining its effect on inflammation, immunity, and chronic organ damage.

In this study, we hypothesized that changes in the gut microbiota during organ transplantation and the associated antibiotic and immunosuppressive therapies critically affect graft outcome. The current study dissected the interactions between the enteric microbiota and innate and adaptive inflammation and immunity in a cardiac transplantation model. Our study showed that both proinflammatory and antiinflammatory microbiota populations, as well as specific bacterial strains, can be defined by their effects on the long-term outcome of the grafts. The mechanistic exploration suggested differential stimulation of myeloid cells (i.e., macrophages and DC) by microbiota, resulting in changes in lymph node (LN) structure that ultimately influence allogeneic immunity.

Results

Differences in gut microbiota composition of normal, colitic, and pregnant mice

To assess the impact of different characteristics of the gut microbiota on organ transplant outcome, we developed a murine organ transplantation model, in which recipients also underwent fecal microbiota transplants (FMT) to alter their gut microbiota. Transplanted stool samples were obtained from normal, pregnant, or colitic donor mice. Since pregnancy is an antiinflammatory environment promoting immunological tolerance to the developing fetus, we hypothesized that stool from pregnant mice would be antiinflammatory and prolong graft survival (21). We also hypothesized that spontaneously colitic mice that lacked the normal complement of Tregs (22, 23) would have a proinflammatory environment without compensatory suppressive mechanisms and that stool from these mice would be proinflammatory and detrimental to allograft survival (24).

We initially characterized the differences in microbiota composition in normal, pregnant, and colitic mice using 16S rRNA gene sequencing. A total of 297,959 sequences from 15 samples (5 mice/group; 19,863.9 ± 3,655.3 on average per sample) were clustered into 3,600 operational taxonomic units (OTUs) assigned to 88 different bacterial genera. Comparison of the community structures using α-diversity (Shannon diversity index) revealed significantly lower bacterial diversity in normal vs. colitic microbiota ($P = 0.014$) (Figure 1A). Although not statistically significant, the Shannon diversity index of the pregnant gut microbiota tended to be higher compared with normal mice (4.15 vs. 3.56, respectively). β-Diversity comparison of overall bacterial community structures using Jensen–Shannon similarity revealed significant differences (ANOSIM, $P = 0.001$), with data points clustering separately (Figure 1B). Comparison of the top 25 genus-level taxa revealed significant compositional differences using DeSeq2 and a P value cutoff of 0.05 (Figure 1C). Among these differences, the normal and pregnant microbiotas were characterized by higher relative abundance of *Lactobacillus* and *Bifidobacterium*, whereas the colitic

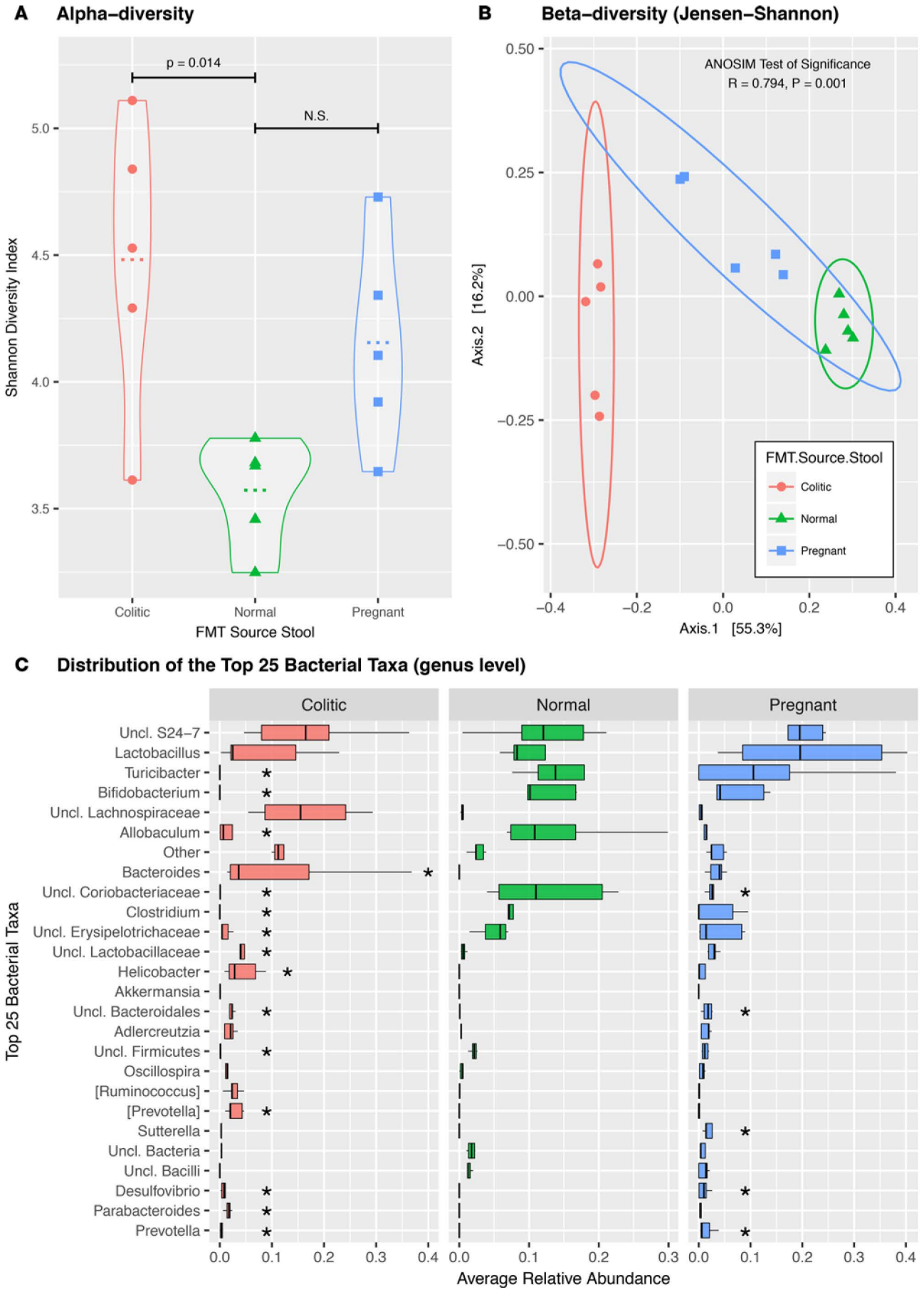
A Alpha–diversity
p = 0.014
N.S.
Shannon Diversity Index
5.0
4.5
4.0
3.5
Colitic
Normal
Pregnant
FMT Source Stool
B Beta–diversity (Jensen–Shannon)
ANOSIM Test of Significance
R = 0.794, P = 0.001
Axis.2 [16.2%]
0.50
0.25
0.00
−0.25
−0.50
−0.4
−0.2
0.0
0.2
0.4
Axis.1 [55.3%]
FMT.Source.Stool
Colitic
Normal
Pregnant
C Distribution of the Top 25 Bacterial Taxa (genus level)
Colitic
Normal
Pregnant
Top 25 Bacterial Taxa
Uncl. S24−7
Lactobacillus
Turicibacter
Bifidobacterium
Uncl. Lachnospiraceae
Allobaculum
Other
Bacteroides
Uncl. Coriobacteriaceae
Clostridium
Uncl. Erysipelotrichaceae
Uncl. Lactobacillaceae
Helicobacter
Akkermansia
Uncl. Bacteroidales
Adlercreutzia
Uncl. Firmicutes
Oscillospira
[Ruminococcus]
[Prevotella]
Sutterella
Uncl. Bacteria
Uncl. Bacilli
Desulfovibrio
Parabacteroides
Prevotella
0.0
0.1
0.2
0.3
0.4
Average Relative Abundance

Figure 1. Characterization of differences in the gut microbiota structure and composition of fecal microbiota transplant (FMT) source samples from normal, colitic, and pregnant mice. (**A**) Violin plot of α-diversity (Shannon diversity index). Shannon was significantly lower in normal vs. colitic mice (Tukey's HSD, $P = 0.014$). (**B**) Principal Coordinate Analysis (PCoA) plots of Jensen–Shannon divergence computed on Cumulative Sum Scaling–normalized (CSS-normalized) datasets between gut microbiota FMT source samples. Ellipses represent the 95% CI by FMT source sample. ANOSIM testing revealed significantly different clusters between the 3 FMT source groups ($R = 0.794$, $P = 0.001$). (**C**) Box plots showing the distribution of the top 25 genus-level bacterial taxa across the 3 FMT groups. Hinges represent the first and third quartiles, with the second quartile (median) displayed by the black line inside each box; whiskers denote the 1.5 interquartile range. Asterisks denote significant differential relative abundance (DESeq2 at level $P < 0.05$) of taxa compared between colitic or pregnant to normal source FMT samples. $n = 5$ for each FMT group.

microbiota was characterized by higher relative abundance of *Lachnospiraceae* (unclassified at the genus level), *Bacteroides*, *Desulfovibrio*, and *Mucispirillum*.

The gut microbiota influences acute graft rejection

To determine if the composition of gut microbiota influenced cardiac transplant outcome, we exposed C57BL/6 (H-2^b) mice to broad spectrum antibiotics for 6 days ad libitum in drinking water, a regimen that depleted endogenous microbiota (25). On day 0, after 24 hours without antibiotics, these antibiotic-treated recipients were transplanted with complete MHC mismatched, allogeneic BALB/c (H-2^d) hearts. These recipients also underwent FMT via orogastric lavage, using pooled stool samples obtained from normal, pregnant, or colitic donor mice. In initial control groups, graft survival after antibiotic treatment alone (median 7 days; mean 7.9 ± 0.7 days) and antibiotic treatment plus normal FMT (median 9 days; mean 10.2 ± 0.7 days), pregnant FMT (median 11 days; mean 10.6 ± 0.2 days), or colitic FMT (median 10 days; mean 9.5 ± 0.5 days) were not different from one another (Figure 2A). Therefore, antibiotics alone or antibiotics plus a variety of FMTs did not influence graft survival. These results were anticipated in the setting of the strong immunologic disparity of a full MHC mismatch without any additional immunosuppression. Thus, unlike gnotobiotic mice that have underdeveloped immune systems and that undergo acute immune activation when exposed to even normal microbiota (16), these recipients had fully developed immune systems with prior and current exposure to normal microbiota.

To promote early graft survival, additional groups of mice underwent antibiotic treatment, cardiac transplantation, and FMT and also received a single dose of 250 μg of anti-CD40L mAb to provide transient immunosuppression. We considered this to be a model of acute rejection due to the transient presence of induction immunosuppression. Antibiotics alone resulted in rapid rejection, as expected; and anti-CD40L mAb alone also resulted in mildly delayed rejection because a single dose of anti-CD40L mAb provided only some immunosuppression (Figure 2B) (26). In contrast, antibiotics plus anti-CD40L mAb resulted in more prolonged graft survival, suggesting that antibiotics could ablate some microbiota components that were detrimental to graft survival (Figure 2B) (16). The combination of antibiotics, anti-CD40L mAb, and either normal or pregnant FMT also resulted in enhanced survival (Figure 2B). In contrast, colitic FMT in this regimen reduced graft survival in comparison with the normal or pregnant FMT and anti-CD40L groups (Figure 2B).

Overall, the addition of transient immunosuppression revealed a graft survival advantage for recipients of antibiotics or pregnant FMT plus antibiotics, compared with no antibiotics or antibiotics plus colitic FMT. These results suggest that microbiota had both positive and negative influences on allograft survival. Importantly, these pilot experiments validated our study design and hypothesis that shifts in the gut microbiota impact graft survival.

The gut microbiota influences chronic graft rejection

These initial experiments represented a model of acute rejection due to transient immunosuppression. However, organ transplant rejection and IF/TA in human recipients is often characterized by slow chronic inflammatory processes, despite the continued presence of maintenance immunosuppression, leading to allograft dysfunction and loss. Therefore, we next assessed the effects of FMT in a more clinically relevant model of chronic immunosuppression and rejection, where C57BL/6 mice again received antibiotics from day –6 to –1, were then transplanted with BALB/c hearts on day 0, and received FMT from normal, pregnant, or colitic donors via gavage on day 0. These recipients also received tacrolimus (2 mg/kg/d s.c.) from day 0 until graft rejection or up to a maximum of 40 days. This amount was chosen to be in the low- to mid-range dose for prolongation of murine organ transplants (27, 28). Recipients were euthanized on the day of rejection or day 40 — whichever came first.

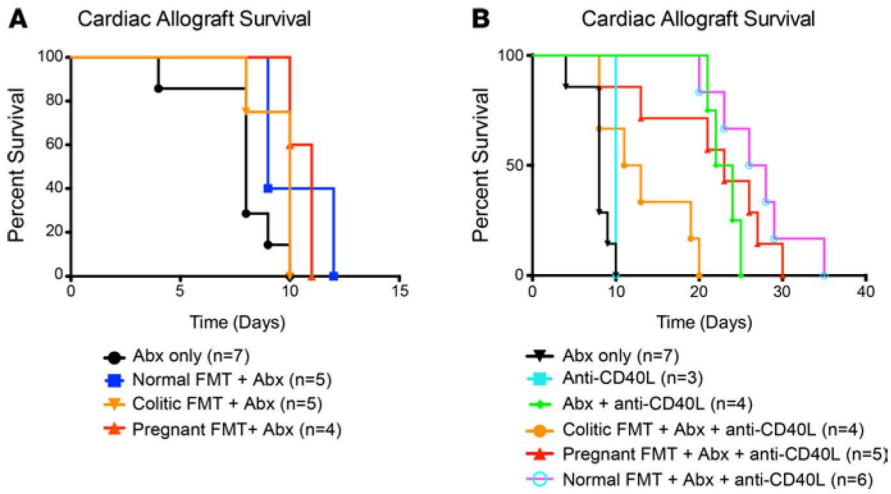

Figure 2. Allograft survival after fecal microbiota transplant (FMT) in acute graft rejection. C57BL/6 recipients transplanted with BALB/c hearts were administered FMT from normal, pregnant, or colitic donors and received (**A**) no immunosuppression or (**B**) 250 μg anti-CD40L mAb. In the absence of immunosuppression (**A**), there was no statistical difference between the FMT groups. For the anti-CD40L mAb–treated group (**B**): anti-CD40L vs. abx + anti-CD40L, $P = 0.0143$; anti-CD40L vs. normal FMT + abx + anti-CD40L, $P = 0.0047$; anti-CD40L vs. pregnant FMT + abx + anti-CD40L, $P = 0.0436$; and anti-CD40L vs. colitic FMT + abx + anti-CD40L, $P = 0.2637$. There was no statistical difference between the pregnant FMT + abx + anti-CD40L, normal FMT + abx + anti-CD40L, and abx + anti-CD40 groups. Log-rank comparisons.

Graft survival and histology. The pregnant FMT group had no graft failures, and survival in this group was significantly longer than in the normal FMT group (Figure 3A). To determine if FMT also influenced allograft histology and inflammation, cardiac grafts were analyzed by histology. Inflammation scores (Figure 3B) were derived by combining a parenchymal rejection score based on H&E-stained sections (Figures 3, C–E) and a fibrosis score based on Masson's trichrome–stained sections (Figures 3, F–H). Recipients of pregnant FMT had significantly lower combined graft inflammation scores than recipients of either normal ($P = 0.02$) or colitic FMT ($P = 0.01$) (Figure 3B). Thus, pregnant FMT was also protective for graft inflammation during chronic immunosuppression and rejection. The scores in the colitic group were higher than those in the normal FMT group but did not reach statistical significance.

Bacterial community composition using 16S rRNA gene sequencing. Since differences in microbiota input influenced graft survival and inflammation over the long term, we determined if structural and compositional differences of donor stool samples persisted over time in the recipients and if these differences associated with graft survival. Microbiota were characterized using 16S rRNA gene sequencing of stool samples collected throughout the experiment. A total of 727,116 sequences across 42 samples (17,312.3 ± 7,489.1 sequences on average per sample) were clustered into a total of 3,934 OTUs.

We previously showed significant differences in bacterial community structure and composition of normal, colitic, and pregnant donor samples. Following FMT, the gut microbiota of recipient mice remained distinct over time and clustered by FMT group even after 40 days (Figure 4A) (ANOSIM, $R = 0.6328$, $P = 0.001$). High-dimensional class comparisons using linear discriminant analysis of effect size (LEfSe) showed that bacteria belonging to the *Bifidobacterium* genus, as well as 2 other OTUs unclassified at the genus level (one OTU belonging to the *Bacilli* class, and another belonging to *Clostridiales* order) were significantly associated with the improved graft outcome in the pregnant FMT group (Figure 4B). Using standard bioinformatics pipelines, bacterial taxonomic assignments from 16S rRNA gene sequencing datasets can generally only be performed to the genus level, and additional analyses are required for species-level assignments. To narrow down the specific species of *Bifidobacterium* significantly associated with the pregnant FMT transplant outcome, *Bifidobacterium* OTU sequences were aligned with *Bifidobacterium* reference sequences, and the resulting phylogenetic tree (Supplemental Figure 1; supplemental material available online with this article; https://doi.org/10.1172/jci.insight.121045DS1) showed that the *Bifidobacterium* OTUs clearly clustered within the *Bifidobacterium pseudolongum* (*B. pseudolongum*) species. Therefore, the *B. pseudolongum* species was used in subsequent experiments below, aimed at further characterizing the protective effect of pregnant stool FMT on transplant outcome.

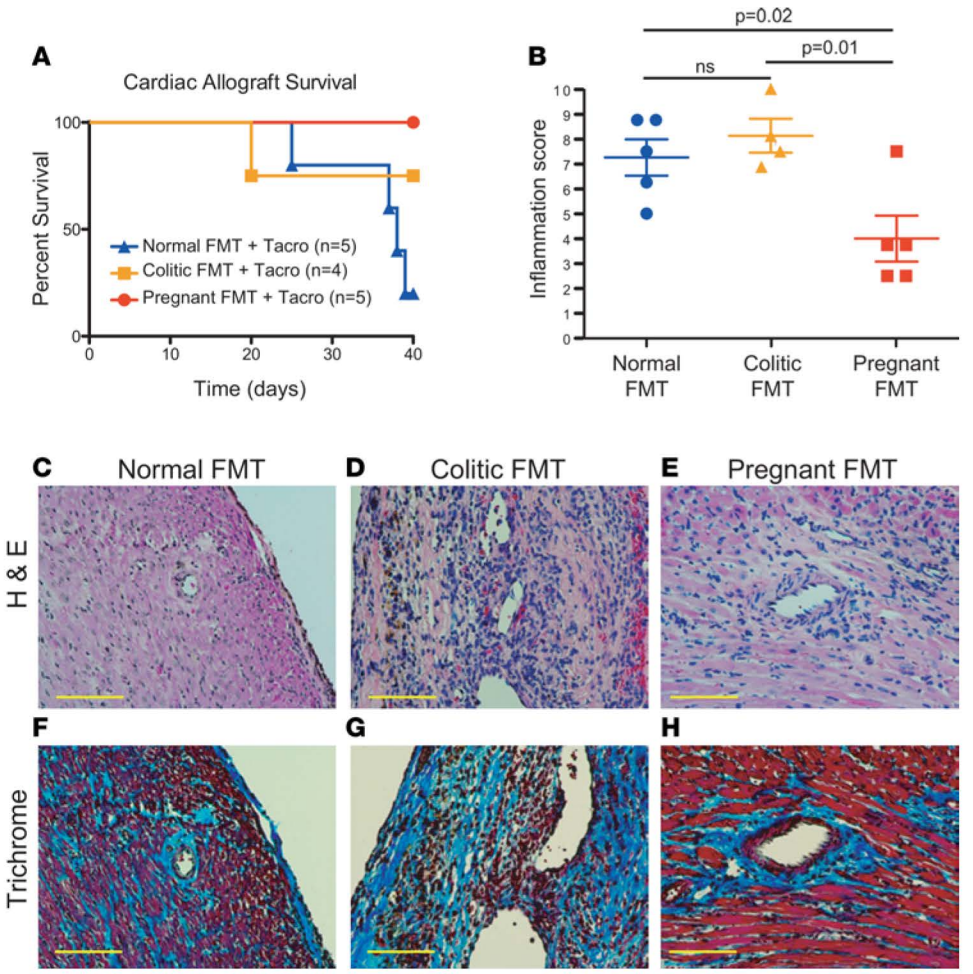

Figure 3. Allograft survival after fecal microbiota transplant (FMT) in chronic graft rejection with tacrolimus 2 mg/kg. C57BL/6 recipients transplanted with BALB/c hearts were administered antibiotics (abx) followed by FMT from normal, pregnant, or colitic donors, and received tacrolimus 2 mg/kg/d s.c. for up to 40 days. (**A**) Survival curve. Allograft survival was significantly improved in FMT with pregnant donor compared with normal ($P = 0.013$). Log-rank comparisons. (**B**) Summary of histology results from **C–H**. Three tissue sections/graft; 2 fields/section. Two-tailed unpaired Student's *t* tests. (**C–H**) Photomicrographs of H&E- and trichrome-stained graft sections from indicated treatment groups in **B**. Scale bars: 100 μm.

The LEfSe analysis also showed that bacteria belonging to the *Mucispirillum* and *Desulfovibrio* genera were significantly associated with worst graft survival outcome in the colitic FMT group (Figure 4B). *Mucispirillum* and *Desulfovibrio* have previously been identified as biomarkers of active colitis, significantly enriched in human and murine colitogenic gut microbiomes (24, 29, 30). Analysis of the relative abundance of these taxa over time following FMT and organ transplant showed that *Bifidobacterium* remained abundant in pregnant FMT samples for at least 40 days (Figure 5A). In contrast, *Desulfovibrio* remained more abundant in colitic FMT samples compared with pregnant FMT samples for up to 2 weeks following transplant ($P < 0.05$, 2-tailed unpaired Student's *t* test comparing pregnant vs. colitic samples at week 2), after which there was an increase in relative abundance in colitic FMT samples, but that was not significantly different from the other FMT groups (Figure 5B).

These experiments revealed highly significant differences in the bacterial community structures and composition of normal, colitic, and pregnant FMT source fecal samples, which in turn affected FMT recipients and cardiac transplant outcome (survival and histopathology). Bacteria assigned to the *B. pseudolongum* species were present in relatively high abundance in pregnant FMT source samples and persisted within the gut microbiota of pregnant FMT recipients. These bacteria were highly significantly associated with a lower inflammation in the transplanted organ, indicating a potential antiinflammatory effect of these bacteria, possibly affecting both innate and adaptive immunity, and revealing an impact of the local or regional

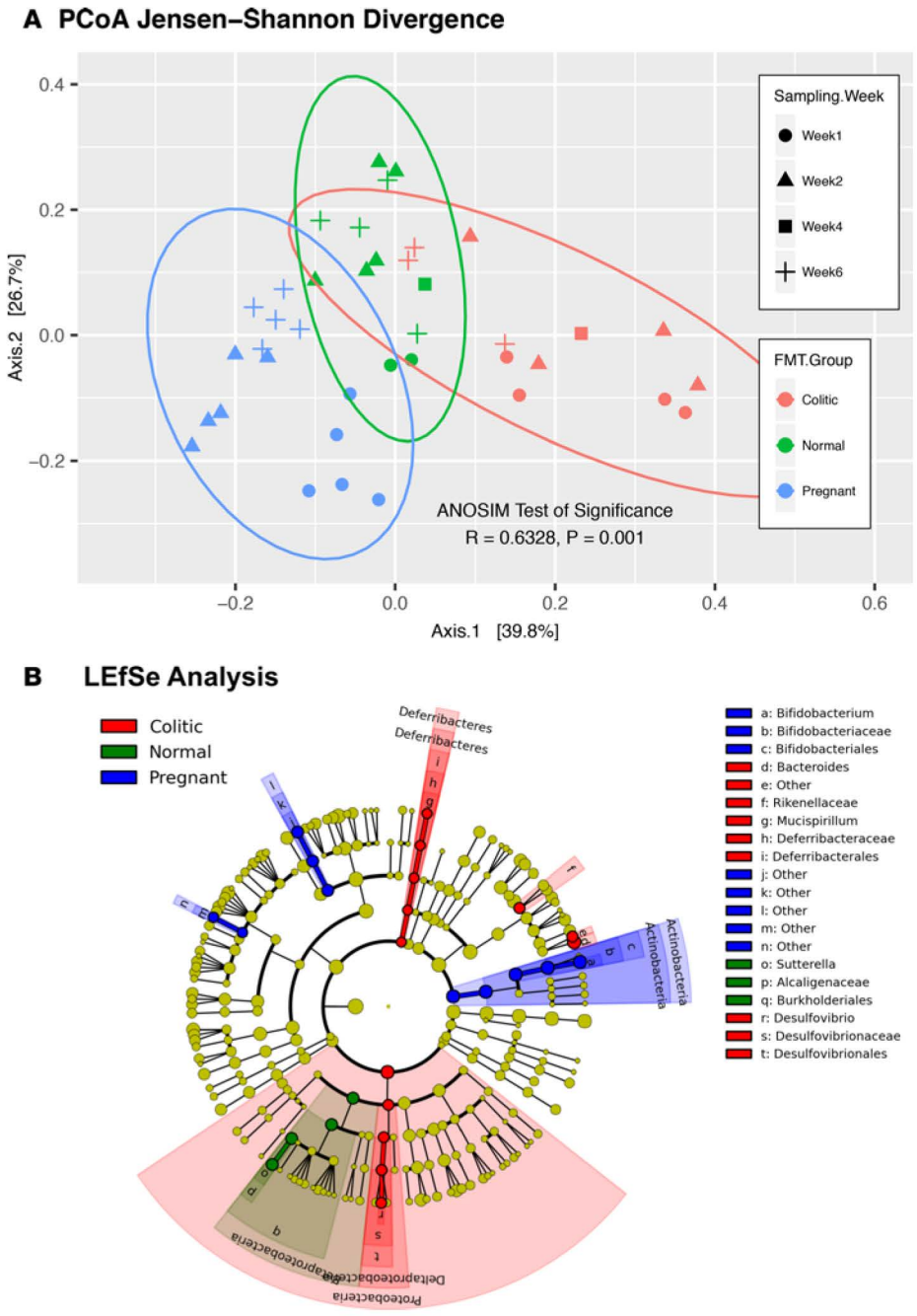

Figure 4. Gut bacterial communities following fecal microbiota transplant (FMT) in chronic graft rejection. Microbiota characterization was performed on samples collected up to day 40 or rejection in C57BL/6 allograft recipients following FMT with normal, pregnant, or colitic donors. (**A**) Principle coordinate analysis (PCoA) plot of Jensen–Shannon divergence computed on CSS-normalized datasets between gut microbiota samples from normal (green), colitic (red), and pregnant (blue) FMT groups. Ellipses represent the 95% CI. (**B**) LEfSe analysis of data points from normal, colitic, and pregnant gut microbiota FMT groups.

gut microbiota on systemic immunity and allograft outcome. Other bacterial species were associated with proinflammatory effects. However, these experiments alone could not prove whether *B. pseudolongum* alone could induce the amelioration of cardiac allograft survival and histology.

B. pseudolongum alone improves transplant outcome. The experiments above using tacrolimus at a dose of 2 mg/kg/d associated *B. pseudolongum* as a likely candidate for the protective effect of pregnant FMT. In order to assess whether shifts in the entire gut microbiota were required for improved cardiac allograft survival and chronic immunosuppression, or if a single bacterial species could — on its own — trigger these effects, follow-up transplant experiments were performed using *B. pseudolongum* ATCC25526 alone via oral gavage following antibiotic treatment. In addition, and since there were some graft failures at the 2 mg/kg/d tacrolimus dose, the dose was increased to 3 mg/kg/d to more fully reproduce clinically relevant chronic immunosuppression and rejection and to focus the evaluation on graft histology and inflammation. Recipients were followed for a longer time and were euthanized on the day of rejection or day 60 — whichever came first.

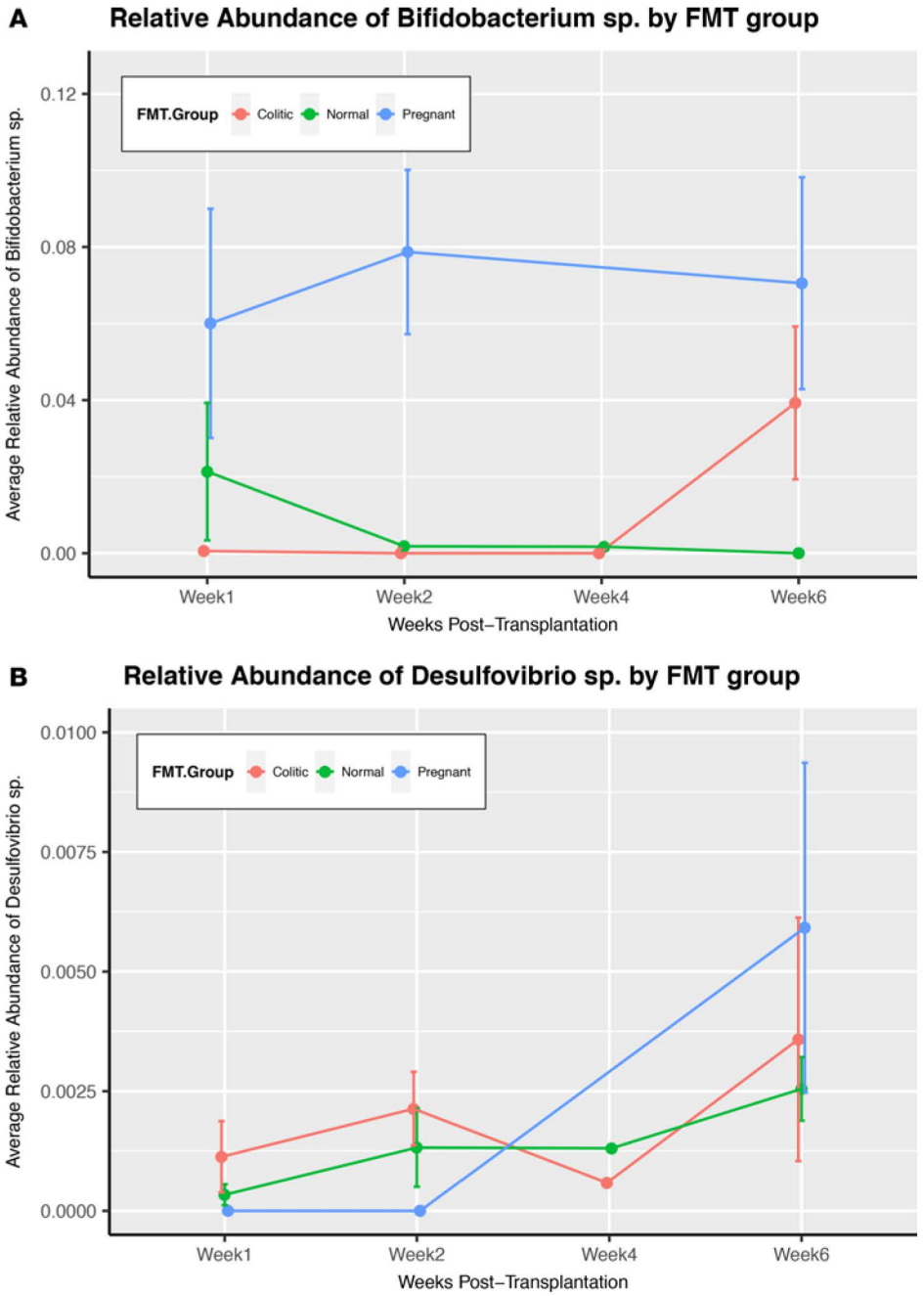

Figure 5. Shifts in the relative abundance of *Bifidobacterium spp.*and *Desulfovibrio spp.* following fecal microbiota transplant (FMT) in chronic graft rejection. Microbiota characterization was performed on samples collected up to day 40 or rejection in C57BL/6 allograft recipients following FMT with normal, pregnant, or colitic donors. (**A**) Relative abundance over time of *Bifidobacterium spp*. operational taxonomic units (OTUs) over time. Significance (2-tailed unpaired Student's *t* test): week 2, pregnant vs. normal, $P < 0.01$; week 2, pregnant vs. colitic, $P < 0.05$. (**B**) Relative abundance of *Desulfovibrio* OTUs over time. Significance (2-tailed unpaired Student's *t* test): week 2, pregnant vs. colitic, $P < 0.05$.

Graft survival and histology. There were no significant differences in survival among the 4 groups (Figure 6A), which was anticipated since this model more fully resembled chronic immunosuppression and rejection with the slightly increased dose of tacrolimus. There were low to moderate levels of alloantibody in these recipients, and there were no differences among the 4 groups for the presence of serum alloantibodies at 14, 28, or 60 days or at the day of rejection (Figures 6, B–D). One of the 2 grafts that rejected in the colitic FMT group was accompanied by a very high alloantibody response at day 14 and the day of rejection. The recipients of both pregnant FMT and *B. pseudolongum* had lower combined graft inflammation scores than recipients of either normal or colitic stool (Figure 6). Thus, both FMT with pregnant stool source and gavage with *B. pseudolongum* were protective for graft inflammation. It is important to note that *B. pseudolongum* ATCC25526 is a human isolate and not mouse adapted yet was active in this in vivo assay. These data show the relevance of a murine assay for human microbiota. It will be interesting in future investigations to use murine-adapted or -derived species. It is also important to note that gavage was performed using purified bacteria and not along with other normal microbiota or encased within fecal matter, all of which could be protective for survival of bacteria in the stomach and proximal small intestine.

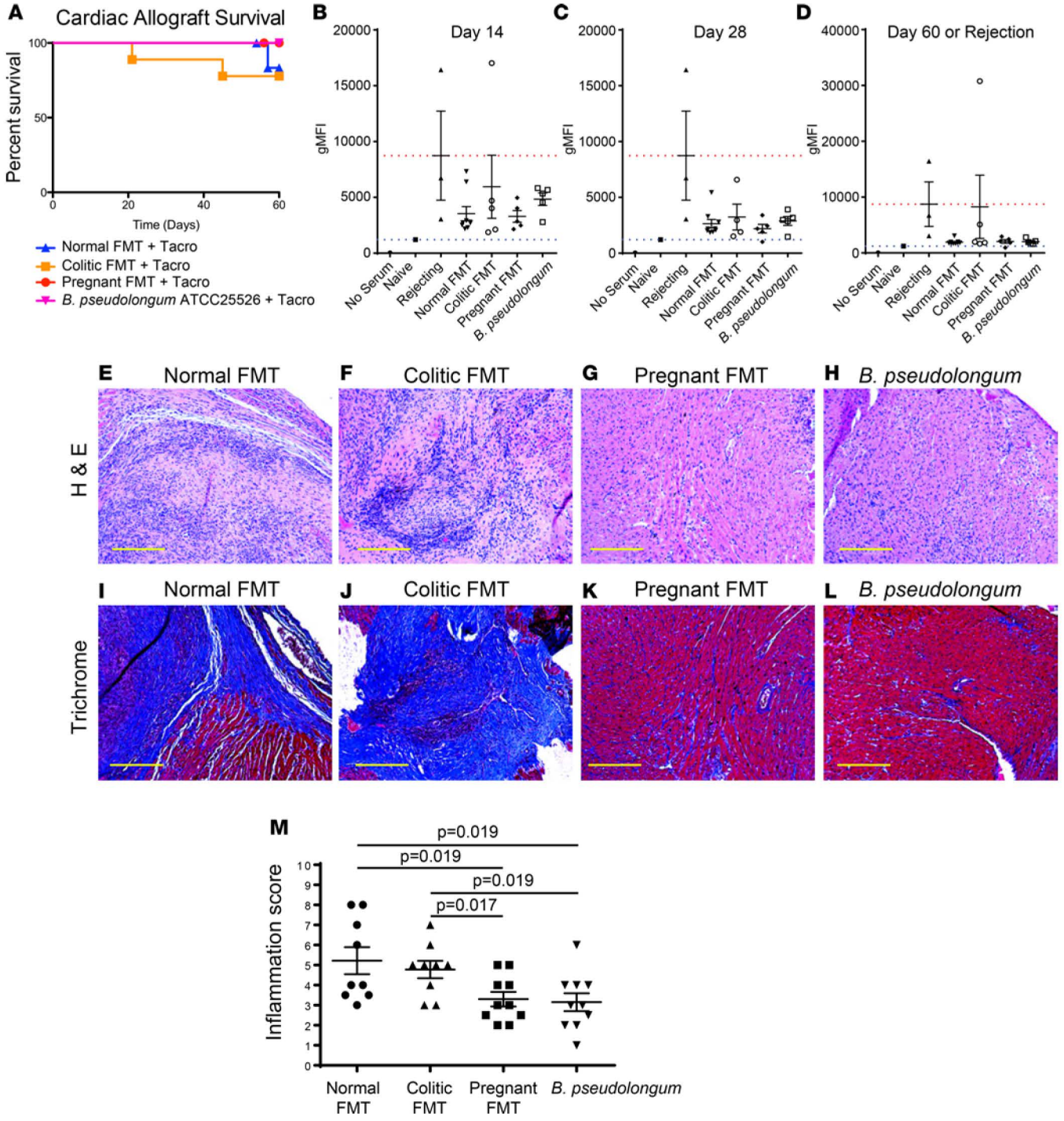

Figure 6. Allograft survival after fecal microbiota transplant (FMT) in chronic graft rejection with tacrolimus 3 mg/kg. C57BL/6 recipients were given antibiotics from day –6 to –1 and on day 0 transplanted with BALB/c hearts; were administered FMT from normal, pregnant, or colitic donors or *B. pseudolongum*; and received tacrolimus 3 mg/kg for up to 60 days. n = 9–10 mice/group. (**A**) Survival curve. Log-rank comparisons. (**B–D**) Alloantibody results at indicated time points. Geometric mean fluorescence intensity (gMFI). Groups compared via Tukey post hoc tests of 1-way ANOVA. (**E–L**) Photomicrographs of H&E- and trichrome-stained graft sections from indicated treatment groups. Scale bars: 200 μm. (**M**) Summary of histology results from **E–L**. Three tissues sections/graft; 2 fields/section. Unpaired 2-tailed Student's t tests.

Microbiota alter regional and systemic LN structure

The microbiota induces direct local effects on the intestinal epithelium and associated leukocytes of the epithelium and lamina propria. These local effects are rapidly dispersed into regional and systemic changes in the immune system, due to migration of both innate and adaptive leukocyte subsets (31–33).

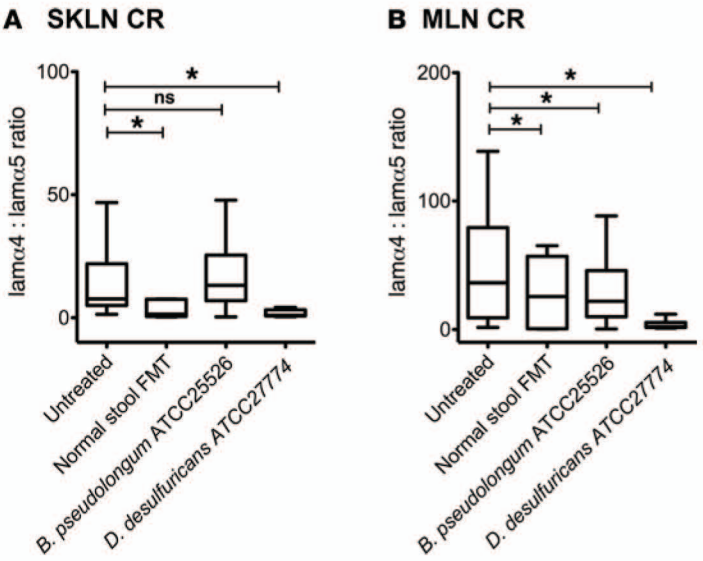

Figure 7. Antibiotics and fecal microbiota transplant (FMT) alter mesenteric and skin draining lymph node (LN) structure. C57BL/6 mice were treated with the antibiotic regimen for 6 days, rested for 1 day, and then received the indicated FMT or a single bacterial strain (1×10^7 CFU). Two weeks later, mesenteric and skin draining LN (MLN and SKLN, respectively) were harvested and assessed by quantitative IHC for laminin α4 and α5 expression and ratios around the cortical ridge (CR). Three mice/group, 3–4 MLN/mouse, 3–4 SKLN/mouse, 3 sections/LN, and 10 fields/section. Dunnett's multiple comparisons test of 1-way ANOVA.

We demonstrated above that the microbiota influenced graft outcomes of survival, inflammation, and fibrosis. To further link the local effects on innate immunity and the systemic effects on graft outcome, we investigated the effect of the microbiota on mesenteric and peripheral skin-draining LN structure. We previously demonstrated that LN structure and function were critical determinants of alloantigen-specific T cell migration, differentiation, and function (34–36). We and others also demonstrated that both adaptive and innate immunity determine LN structure, function, and remodeling and the outcomes of graft survival (37–42). In particular, we discovered that the expression ratios of laminin α4 and α5 in the LN cortical ridge and surrounding the high endothelial venules, the portals of entry of cells into the LN, determined T cell migration and differentiation to regulatory versus effectors cells (43). Specifically, a high laminin α4/α5 ratio was protolerogenic, while a low laminin α4/α5 ratio was inflammatory and immunogenic.

Groups of mice were treated with the antibiotic regimen for 6 days and then received a single FMT of normal stool or were gavaged with *B. pseudolongum* or *D. desulfuricans* ATCC2774. After 2 weeks, the animals were euthanized, mesenteric and peripheral (axillary, inguinal, popliteal, brachial) LNs were harvested, and laminin α4 and α5 expression was assessed. The results showed that antibiotic treatment followed by FMT with normal stool resulted in a decrease in the cortical ridge laminin α4/α5 ratios of both mesenteric and skin-draining LN compared with untreated controls not receiving antibiotics or FMT (Figure 7). Importantly, *B. pseudolongum* ATCC25526 administration resulted in higher cortical ridge laminin α4/α5 ratios of both mesenteric and skin-draining LN compared with normal stool FMT. In contrast, treatment with *D. desulfuricans* resulted in extremely low ratios for all measures. These results demonstrated that antibiotics and either FMT or single-strain bacterial transfer resulted in both regional and systemic changes in LN structure. These changes were commensurate with effects on myeloid cell responses and outcomes of allografts. These results support the hypothesis that the microbiota had significant and long-term effects on innate immunity, and LN structure and function, that determine subsequent adaptive regional and systemic immune events (44).

As noted above, cytokines and innate cells such as DC and macrophages are known to be intimately involved in regulating LN remodeling. Microbiota directly interact with many immune cells — particularly myeloid cells of the innate immune system (9, 10, 15). Innate immunity, in turn, has downstream effects on adaptive immunity and the response to alloantigen (11, 16, 17). Therefore, we determined if *B. pseudolongum* or *Desulfovibrio* bacteria could stimulate myeloid cells and if myeloid responses reconciled with the observed immune effects on LN and allograft histology. The RAW264.7 macrophage and the JAWSII DC

lines were directly stimulated in vitro with UV-killed bacteria. The stimulation included *B. pseudolongum* ATCC25526, which was compared with *D. desulfuricans* ATCC2774, and LPS as a positive control. Pilot experiments with cytokine transcript arrays and reverse transcription PCR (RT-PCR) showed differences in the responses of the cell lines to the diverse microbial stimuli (data not shown). These responses were then confirmed at the translational level by ELISA assays (Supplemental Figure 2). The results showed that *D. desulfuricans* induced high levels of IL-6 and TNFα in both the macrophage and DC lines (Supplemental Figure 2A and Supplemental Figure 2B). In contrast, *B. pseudolongum* induced low levels of IL-6 in RAW264.7 (Supplemental Figure 2A) and induced no or lower levels of TNFα in the 2 cell lines.

All bacteria induced expression of the homeostatic chemokine CCL19 from both cell lines. *B. pseudolongum* maintained an IL-10 response in the macrophage line, while *D. desulfuricans* inhibited IL-10 production and LPS induced a very high IL-10 response. *B. pseudolongum* also induced an IL-10 response in the DC line, while *D. desulfuricans* induced a much greater response. While IL-10 is often considered to be an immunosuppressive cytokine, it induces substantial stimulation of some cell subsets, particularly at higher doses (45).

Overall, *D. desulfuricans* induced stronger inflammatory-type responses in both cell lines, with increased production of IL-6 and TNFα compared with *B. pseudolongum*. *B. pseudolongum*–induced responses were more notable for homeostatic CCL19 and antiinflammatory IL-10. There is evident complexity in these responses. As noted above, the *B. pseudolongum* ATCC25526 strain is human derived and not murine adapted. The *D. desulfuricans* ATCC27774 strain is isolated from the sheep rumen. There are also differences between macrophage and DC line responses to the same stimuli. Additional work will be required to understand kinetics, doses, response of primary cells rather than immortalized lines, and in vivo responses to confirm and extend these findings.

Discussion

Gut microbiota populations and individual bacterial strains profoundly influenced the outcomes of vascularized cardiac allografts in a clinically relevant murine model involving antibiotic administration, conventional chronic immunosuppression, and complete MHC mismatching. FMT using source stool samples from pregnant mice or gavage with isolated *B. pseudolongum* species resulted in improved long-term allograft survival and prevention of inflammation and fibrosis in the grafts. In contrast, FMT using source stool samples from colitic or normal mice resulted in markedly worse graft outcomes. Mechanistic investigations of innate immune responses revealed that *B. pseudolongum* induced more balanced antiinflammatory and homeostatic cytokine responses from DC and macrophages compared with *D. desulfuricans* bacteria. Further analysis revealed diametrical effects of these bacteria on LN structure, with *B. pseudolongum* inducing a cortical ridge laminin α4/α5 ratio associated with suppression and tolerance, while *D. desulfuricans* induced a laminin α4/α5 ratio associated with inflammation and allograft rejection. These results strongly supported our hypothesis that microbiota populations, and even single bacterial species, influenced allograft outcomes and alloimmunity through broad effects on the local, regional, and systemic innate and adaptive immune systems.

Antibiotics alone did not influence early acute allograft survival in our model. This result was expected, given the complete MHC mismatch between donor and recipient with a strong allogeneic response. Lei et al. (16) showed improvement in allograft survival with the use of antibiotics alone; notably, their model used minor histocompatibility mismatches or employed gnotobiotic mice, which undergo significant immune stimulation when initially exposed even to normal microbiota. We observed significant changes in LN laminin α4/α5 ratios in mice treated only with antibiotics and normal FMT. This suggested that antibiotic treatment had detrimental and persistent effects on the immune system. Our observations are commensurate with those showing that antibiotic treatments have long-term effects on microbiota structure (10, 19, 46–48) and that inflammatory events that originate from the microbiota persist as long-term changes in secondary lymphoid organ structure and function (44). Future investigations will more closely detail the kinetics and persistence of LN structural changes as a result of antibiotic administration with or without FMT interventions.

In an attempt to characterize the murine intestinal gene expression profiles associated with either pro- and antiinflammatory outcomes, we performed transcriptomic analyses of tissue samples along the gastrointestinal tract (small intestine, caecum, and colon), obtaining on average 92,000,000 reads per sample, with approximately 42% of the reads in each sample mapping to the murine genome. Hierarchical clustering showed no differences of overall gene expression between the different study groups

(Supplemental Figure 3A), and multi-dimensional scaling (MDS) analysis also revealed no clear clustering (Supplemental Figure 3B). Differential gene expression analysis (edgeR, upper quartile, FDR = 0.1) comparing high- vs. low-inflammation score samples identified only 9 genes as significantly upregulated in high-inflammation intestinal samples (Supplemental Table 3): 4 genes with unknown function and Hba-a2 (gene coding for the hemoglobin α, adult chain 2), Muc5ac (gene coding for mucin 5, subtypes A and C), Ighv2-4 and Ighv4-1 (genes coding for immunoglobulin heavy variable regions), and Sox1ot (gene coding for the Sox1 overlapping transcript). This lack of significantly differentially abundant genes beyond 60 days after FMT and organ transplant strongly suggests that pro- or antiinflammatory signals are likely to be very early events happening soon after transplantation and that they do not persist locally in the intestinal epithelium. Future investigations focusing on the early inflammatory events immediately following transplantation will more closely detail the kinetics and persistence

The changes induced here by oral antibiotics and FMT in the intestinal microbiota were later manifested in regional and system changes to LN structure and to distant changes in allograft inflammation, fibrosis, and survival. Others have shown that local and regional changes in microbiota and immune interactions in the intestinal mucosa, submucosa, lamina propria, and proximal LN can be rapidly translated into regional and system immune modulation (31, 32, 44, 49, 50). Our studies showed that the gut microbiota stimulated different myeloid cell innate immune responses and influenced proximal and distal LN structure. These observations suggest the hypothesis that microbiota-stimulated innate immune cells could secrete cytokines and chemokines and/or migrate to the LNs in order to shape stromal structures. It will be important to define which myeloid cells are most influenced in vivo by these microbiota with pro- or anti-inflammatory characteristics, or by individual bacterial isolates, and how myeloid cells directly or indirectly regulate downstream LN structure.

As noted above, we and others demonstrated that innate and adaptive immunity regulate LN structure, remodeling, and dynamics (34–43). In particular, the laminin α4/α5 ratio determined the entry of T cells into the LN and their fate toward immunity and inflammation versus suppression, tolerance, and $Foxp3^+$ Tregs. The results here extend these findings and show that the microbiota can regulate LN structure which correlates with upstream effects on myeloid cell innate immunity and the downstream effects on graft outcome. It will be important to map the kinetics and persistence of LN remodeling due to both antibiotic and FMT influences. It will be important to directly link specific in vivo myeloid cells and their molecular responses to the changes in LN structure. Lastly, it will be important to understand the trafficking of both alloantigen-presenting DC and alloantigen-responsive T cells to the remodeled LN and how LN structure influences their responses. Preliminary data have shown that laminin α5 directly stimulates CD4 T cell proliferation and differentiation to Th2, and Th17 lineages, while laminin α4 prevents these effects by promoting Treg differentiation (51).

A number of reports document shifts in the microbiota during organ and BM transplantation (16–18, 52–60). Those studies mostly detail associations of microbiota populations with detrimental or beneficial outcomes. The complexity of patient diseases and comorbidities, along with the enormous number of interactions and variables intrinsic to the microbiota, often preclude definitive mechanistic probing of causality. By employing a murine model, we were able to control many variables and move beyond associations of population structure to an outcome event. We identified single bacterial species that have potential to be causal agents, and we then proceeded to test these species for in vitro and in vivo activities. We showed specific effects on myeloid cell responses, LN remodeling, and allograft inflammation and fibrosis. These events provided mechanistic links between specific bacterial members, local innate responses, distant immune organ structure, and adaptive immunity. The links defined specific loci of innate and adaptive immunity that can be probed in further detail to understand how the microbiota influences graft outcomes. Various *Bifidobacterium* species have been associated with numerous immune events in humans (61–64), and human and murine microbiota are often directly comparable (65). Thus, our results strongly support the overarching hypothesis that the human gut microbiota is a major determinant of allograft outcomes and the reason why the long-term results for graft function and survival have not improved.

Numerous studies have demonstrated a critical role of the gut microbiota in the modulation of various aspects of the immune system (11, 15, 49, 50, 66–68). Our studies indicated that discrete bacterial species, such as *B. pseudolongum* or *D. desulfuricans,* triggered anti- or proinflammatory processes with broad consequences to the immune system and the host. Previous studies showed that specific bacterial members of the gut microbiota possessed direct immune-modulating properties. For example, species from the *Lactobacillus*

and *Bifidobacterium* genera possessed beneficial probiotic effects (62, 63, 69–71). However, the precise pathways by which these effects occurred remain elusive. For members of the *Bifidobacterium* genus, exopolysaccharides (EPS), polymers of high-molecular weight mostly composed of polysaccharides and proteins that are expressed at the bacterial cell surface have been the most characterized. Schiavi and colleagues (63) showed that the EPS gene cluster from the commensal *B. longum* strain 35624 was essential in dampening proinflammatory host responses by modulating cytokine secretion and NF-κB activation. Exposure to a *B. longum* 35624 isogenic mutant unable to synthesize the EPS 35624 protein cluster promoted local Th17 responses within the gut and the lung. Salazar and colleagues (62) showed that oral administration of an EPS-producing strain of *B. animalis* was associated with suppression of the proinflammatory cytokine IL-6 and increased synthesis of the regulatory cytokine TGFβ. Fanning et al. (61) characterized the EPS from the human commensal *B. breve* to show that it was linked to the evasion of adaptive B cell responses compared with EPS-deficient mutants and provided protection against infection by a murine pathogen. Other *Bifidobacterium* factors such as the secreted protein serpin, pili, or even DNA have been shown to modulate the local immune environment (72). Dissecting the mechanisms and molecular players underlying the immunomodulatory properties of *Bifidobacterium* will be complicated by interstrain and interspecies diversity (73), reflected in variability in the loci encoding the EPS biosynthesis pathways (74, 75). This cross-species and strain genomic variability is exemplified by comparative genome analyses performed on a *B. pseudolongum* strain that was isolated and sequenced as part of our studies (76), which showed that almost 16% of its genes do not possess any homologs in the previously sequenced *B. pseudolongum* strain PV8-2 genome (GenBank accession number CP007457).

Based on the results from our studies, it is clear that the definition of pro- and antiinflammatory microbiota in the context of organ transplantation will provide a critical platform to define upstream influences that initiate organ inflammation and scarring. Understanding the molecular mechanisms that govern the interplay between the microbiota — or specific bacterial species — and the host system will allow for the development of targeted strategies that should allow for improved prognostic or diagnostic tests in a clinical setting, or even for interventions targeting the microbiota that would promote an environment more favorable to transplant health.

Methods

Supplemental Methods are available online with this article.

Mice. Female C57BL/6 mice were used as cardiac transplant recipients, normal stool donors, and pregnant stool donors. C57BL/6 mice were from the University of Maryland School of Medicine Veterinary Resources breeding colony. Cardiac donors were female BALB/c mice, purchased from The Jackson Laboratory. C57BL/6 and BALB/c mice were used between 8 and 14 weeks of age. TEa T cell receptor transgenic mice (77) on a C57BL/6 background that spontaneously develop colitis, due to a lack of Tregs, were used as the source for colitic stool and were a gift from Alexander Rudensky (Memorial Sloan Kettering Cancer Center, New York, New York, USA) (22, 23).

Cardiac allograft procedure. Sex-matched C57BL/6 mice (10–12 weeks) received heterotopic cardiac allograft transplant from donor BALB/c mice (6–8 weeks) as previously described (78). Graft function was monitored daily by abdominal palpitation. At either time of rejection or 40–60 days after transplant, mice were euthanized and the donor heart was excised, fixed with 10% paraformaldehyde, and embedded in paraffin.

B. pseudolongum and Desulfovibrio desulfuricans bacteria. *B. pseudolongum subsp. pseudolongum Mitsuoka* (ATCC25526) was used in cell stimulation and cytokine assays. *B. pseudolongum* ATCC25526 was initially grown anaerobically at 37°C for 3–5 days on Bifido Selective Media (BSM) agar plates (MilliporeSigma), from which a single colony was selected and grown in BSM broth (MilliporeSigma, 90273-500G-F) until stationary phase (up to 3 days).

Desulfovibrio desulfuricans subsp. desulfuricans (ATCC27774) was grown in Modified Baar's Medium For Sulfate Reducers using the protocol recommended by the ATCC (https://www.atcc.org/~/media/14184D242AA74EC48DF35188A5935BB4.ashx). Cultures were initially incubated under anaerobic conditions for 5 days on Modified Baar's Medium agar plates, after which single colonies were chosen, transferred to liquid media, and incubated for up to 3 weeks.

Eukaryotic cell lines. Both JAWSII immature DC (CRL-11904) and RAW264.7 macrophage (TIB-71) cell lines were purchased from the ATCC. Cells were grown at 37°C, 5% CO_2 in complete culture medium consisting of DMEM (Mediatech Inc.) with 10% FCS (Benchmark) for RAWS264.7 or α minimum essential

medium (Mediatech Inc.) with 20% FCS for JAWSII, supplemented with 4 mM L-glutamine (Lonza), 10 U/ml penicillin and 100 μg/mL streptomycin (Lonza), 1 mM sodium pyruvate (Lonza), and — for JAWSII cells only — 5 ng/ml murine GM-CSF (eBioscience). For JAWSII cells, cultures were maintained by transferring nonadherent cells to a centrifuge tube and treating attached cells with 0.25% trypsin, 0.03% EDTA (Cellgro) at 37°C for 5 minutes, followed by pooling the 2 populations of cells and dispensing them into new flasks at a subculture ratio of 1:2. For RAW264.7 cells, cells were removed from flasks by scraping and distributed to new flasks at a subculture ratio of 1:3 to 1:6. P815 cells (TIB-64, ATCC) were grown in DMEM (Cellgro) supplemented with 10% low IgG FBS (Thermo Fisher Scientific), 2 mM L-glutamine, 100 IU/ml penicillin, and 100 μg/ml streptomycin).

Cell stimulation and cytokine and chemokine assays. D. desulfuricans ATCC 27774 or *B. pseudolongum* cultures were spun down, the supernatant was collected, and bacterial cells were killed by UV exposure at 100 μJ/cm^2 for four 15-minute cycles in a UV CrossLinker. JAWSII and RAWS264.7 cells (1×10^6) were seeded into duplicate 12-well plates in 1 ml complete medium. Twenty-four hours later, the cells were FCS starved with 5% FCS for RAWS264.7 or 10% FCS for JAWSII for 2 hours and then stimulated with LPS, UV-killed *B. pseudolongum* or *D. desulfuricans* bacteria for 24 hours. Culture supernatants were collected for ELISA for the indicated cytokines and chemokines. ELISAs for TNFα, IL-6, and IL-10 were purchased from BioLegend and for CCL19 from Boster Biological Technology.

Source stool collection and FMT. Stool was collected from normal female C57BL/6 mice between 8 and 14 weeks of age, pregnant C57BL/6 mice at approximately days 8–14 of pregnancy, and colitic TEa mice after the onset of colitis (usually 3-–months of age). Pregnant mice were timed using a combination of vaginal plug monitoring, mouse weight tracking, and back-calculation from day of mouse pup birth (C57BL/6 gestation is 19.25 days). Pellets were weighed, homogenized in PBS at 200 mg/ml, and frozen at –80°C until use. Cultured *B. pseudolongum* ATCC25526 bacteria were suspended at 1×10^8 CFU/ml in PBS and used fresh.

For FMT, mice were fed antibiotics (kanamycin, gentamicin, colistin, metronidazole, and vancomycin) ad libitum in drinking water on days –6 to –1 before transplant. On day 0, C57BL/6 mice received BALB/c hearts. Fecal samples (200 μl, 200 mg/ml) or cultured *B. pseudolongum* ATCC25526 (200 μl, 5×10^7 CFU/ml) were also transferred on day 0 by gavage. Mice received daily immunosuppression tacrolimus (2 mg/kg/d s.c. d0-40 or 3 mg/kg/d s.c. d0-60) starting on day 0 (27, 28). Fecal pellets and intestinal tissue were collected from transplanted mice and analyzed via 16S rRNA gene sequencing or RNASeq.

Reagents. Antibiotics were USP grade or pharmaceutical secondary standard: kanamycin sulfate (0.4 mg/ml, MilliporeSigma), gentamicin sulfate (0.035 mg/ml, MilliporeSigma), colistin sulfate (850 U/ml, MilliporeSigma), metronidazole (0.215 mg/ml, MilliporeSigma), and vancomycin hydrochloride (0.045 mg/ml, MilliporeSigma) were dissolved in vivarium drinking water and administered ad libitum. Tacrolimus (USP grade, MilliporeSigma) was reconstituted in DMSO (USP grade, MilliporeSigma) at 20 mg/ml. This stock was diluted to 2–3 mg/kg with absolute ethanol (USP grade, Decon Labs). DMSO/ethanol stock was diluted 1:5 in sterile PBS for s.c. injection and injected at 10 μl/g. Anti-CD40L mAb (clone MR1) grown in serum-free medium was obtain from BioXCell.

Histology. Cardiac allografts were assessed for survival by abdominal palpation; harvested at day 40, day 60, or rejection; fixed for 2 days in 10% buffered formalin (Thermo Fisher Scientific); and transferred to 70% ethanol. Samples were embedded in paraffin and processed and stained with H&E or Masson's trichrome. H&E samples were evaluated for parenchymal rejection score (from 0–4) using previously published criteria (79). Trichrome samples were scored 1–4, with 1 as minimal (<10% area), 2 as mild (10%–30%), 3 as moderate (30%–50%), and 4 as severe (>50%). Slides were read by a single individual blinded to the treatment group of the specimen.

IHC. LN were excised and immediately submerged in OCT compound (Sakura Finetek) or fixed using paraformaldehyde. Sections (5-μm thick) were cut in triplicate using a Microm HM 550 cryostat (Thermo Fisher Scientific) and fixed in cold acetone for 5 minutes, washed in PBS, or left unfixed for fluorescent microscopy. Primary antibodies were diluted between 1:20 and 1:200 in PBS and incubated for 1 hour in a humidified chamber (Supplemental Table 1). Sections were then washed with PBS, and the secondary antibody was applied at a 1:50–1:400 dilution for 30 minutes (Supplemental Table 2). Slides were washed in PBS for 5 minutes, coverslipped, and imaged under a fluorescent microscope, and the images were analyzed with the Volocity software (PerkinElmer).

Transplant-recipient stool collection. Stool pellets were collected fresh from cardiac transplant recipients at 1-week intervals until graft rejection or termination of the experiment. Stool samples were placed in RNA Later (Ambion) in RNAse-free 1.7-ml tubes (Denville), stored at 4°C overnight, and then frozen at –80°C until analysis.

DNA extraction. DNA extraction from mouse stool pellets was adapted from procedures developed at the Institute for Genome Sciences and previously published (80, 81). Negative extraction controls were included to ensure that no exogenous DNA contaminated the samples during extraction. DNA quality control/quality assurance was performed using spectrophotometric measurements on a NanoDrop (Thermo Fisher Scientific), as well as gel electrophoresis.

16S rRNA gene PCR amplification and sequencing. Using a dual-indexing strategy for multiplexed sequencing developed at the Institute for Genome Sciences and described in detail elsewhere (82), the V3V4 hypervariable region of the 16S rRNA gene was PCR amplified and sequenced on the Illumina MiSeq. PCR reactions were set up in 96-well microtiter plates using the 319F (5′ - ACTCCTACGGGAGGCAGCAG - 3′) and 806R (5′ - GGACTACHVGGGTWTCTAAT - 3′) universal primers, each with a linker sequence required for Illumina MiSeq 300bp paired-ends sequencing, and a 12-bp heterogeneity-spacer index sequence to minimize biases associated with low-diversity amplicons sequencing (82, 83). Reactions were performed using the Phusion High-Fidelity DNA polymerase (Thermo Fisher Scientific) and 50 ng of template DNA in a total reaction volume of 25 μl. PCR-negative controls without DNA template were performed for each primer pair. The following cycling parameters were used: 30 seconds at 98°C, followed by 30 cycles of 10 seconds at 98°C, 15 seconds at 66°C, and 15 seconds at 72 °C, with a final step of 10 minutes at 72 °C. Successful amplification was confirmed using gel electrophoresis, after which amplicon cleanup and normalization was performed using the SequalPrep Normalization Plate kit (Invitrogen). A total of 25 ng of 16S PCR amplicons from each sample was pooled, and sequencing was performed using the Illumina MiSeq (Illumina) according to the manufacturer's protocol.

16S rRNA gene sequence processing and analysis. After screening 16S rRNA gene reads for low-quality bases and short read lengths (82), paired-end read pairs were assembled using PANDAseq (84), demultiplexed, trimmed of artificial barcodes and primers, and assessed for chimeras using UCHIME in de novo mode implemented in Quantitative Insights Into Microbial Ecology (QIIME; release v. 1.9) (85). The resulting quality trimmed sequences were then clustered de novo into OTUs with the Greengenes 16S database (v. 13.8) (86) in QIIME (85), with a minimum confidence threshold of 0.97 for the taxonomic assignments. To account for uneven sampling depth and ensure less biases than the standard approach (total sum normalization), data were normalized with metagenomeSeq's cumulative sum scaling (CSS) (87) when appropriate. Taxonomic assignments obtained through QIIME (85) were further analyzed and visualized within RStudio (v. 1.0.143) using the R packages Vegan (88), Phyloseq (89), Bioconductor (90), metagenomeSeq (91), biomformat (92), and ggplot2 (93). Prior to normalization, α diversity (within-sample diversity) was estimated using the Shannon diversity index (94). β-Diversity (between-sample diversity) was determined through principle coordinates analysis (PCoA) plots of Jensen–Shannon divergence distance.

Species-level taxonomic assignment of Bifidobacterium 16S rRNA gene sequences. To narrow the specific species of *Bifidobacterium* significantly associated with the pregnant FMT transplant outcome, 16S rRNA sequences from *Bifidobacterium* OTUs were aligned with *Bifidobacterium* reference 16S sequences from the Ribosomal Database Project (RDP; Release 11, Update 5). A total of 765 full-length sequences (individual isolates with known species, ≥1,200 bp) were initially downloaded and trimmed to V3V4 lengths (V3V4 being the region of the 16S rRNA gene targeted in our sequencing dataset), and nonredundant sequences were removed using CD-HIT (95, 96). The resulting sequence dataset, composed of 111 V3V4 nonredundant *Bifidobacterium* species sequences, was then aligned with sequences representative of *Bifidobacterium* OTUs using ClustalX, and a tree was computed from the ClustX alignment using FastTree (Supplemental Figure 1).

Serum collection. Whole blood was collected into untreated micro-hematocrit glass capillaries (Thermo Fisher Scientific) by tail nicking and allowed to clot at room temperature for 15–30 minutes. The clot was removed by centrifuging at 2,000 *g* for 10 minutes in a refrigerated (4°C) centrifuge. Liquid fraction (serum) was removed and stored at –80°C until assayed.

Alloantibody assay. P815 (H-2^d) mastocytoma cells (1×10^5) were blocked with anti-CD16/32 mAb (clone 93, eBioscience) at 5 μg/ml for 15 minutes at room temperature in 100 μl HBSS/0.5% BSA (MilliporeSigma) in 96-well V-bottom plates (Corning). Mouse serum diluted 1:50 in HBSS 0.5% was

added to wells at 100 μl per well to give a final serum dilution of 1:100. P815 were incubated in serum for 30 minutes at 4°C, washed twice in HBSS/0.5% BSA, and then stained with anti–mouse IgM PE at 0.6 μg/ml (eBioscience, II/41, 12-5790-820) and anti–mouse IgG PE at 1.25 μg/ml (eBioscience, polyclonal, 12-4010-82) for 30 minutes at 4°C. It was then washed twice in HBSS 0.5% BSA, and fixed in 4% paraformaldehyde in PBS (Affymetrix) for 10 minutes at room temperature and washed and resuspended in 200 μl HBSS/0.5% BSA for flow cytometry. Cells were analyzed by flow cytometry using an LSR Fortessa (BD Biosciences), and geometric mean fluorescence index (gMFI) was calculated by FlowJo software (v8.8.7, Tree Star Inc.). Naive mice were used for negative controls, and untreated rejecting recipients were used for positive controls.

Data availability. Sequence data generated in this study was deposited to Genbank and linked to BioProject PRJNA480643 in the NCBI BioProject database (https://www.ncbi.nlm.nih.gov/bioproject/).

Statistics. For 16S rRNA gene sequencing datasets, statistical analyses were performed in R. Significant differences in α-diversity (Shannon diversity) were tested using 1-way ANOVA with Tukey's honestly significant difference (HSD) post hoc test. Differences in β-diversity were assessed using analysis of similarities (ANOSIM) (97) implemented within the R Vegan package on normalized data (999 permutations). Identification of differentially abundant taxa between the different FMT groups was performed using the LEfSe biomarker discovery algorithm, using the Galaxy server (http://huttenhower.sph.harvard.edu/lefse/) (98). Determination of statistically significant differences ($P < 0.05$) in OTU bacterial relative abundance between transplant groups was performed using DESeq2 (99) due to its high power in computing smaller sample sizes (<20 samples per group) (100).

Non-16S datasets were analyzed using GraphPad Prism 7.02 with statistical significance defined for $P < 0.05$. Significance in inflammation scores was tested using 2-tailed unpaired Student's t tests. Comparison of alloantibody titers was performed using 1-way ANOVA with Tukey's post hoc tests. For comparisons of laminin α4/α5 expression ratios, Dunnett's multiple comparisons tests of 1-way ANOVA were used.

Study approval. All the procedures involving mice were performed in accordance with the guidelines and regulations set by the Office of Animal Welfare Assurance of the University of Maryland School of Medicine, under the approved IACUC protocol no. 0715001.

Author contributions

JSB, WFF, and EFM contributed to the study design, protocol development, data analysis, and interpretation. LH, YX, VS, LL, TZ, CW, TS, and CCB conducted the experiments and analyzed the data. EMS contributed to the bioinformatic and biostatistical analyses of the sequencing datasets. JSB and EFM wrote the manuscript.

Acknowledgments

This work was supported by grants from the Living Legacy Foundation of Maryland (EFM and JSB), from the NIH (grant 1RO1AI14496 to JSB), as well as start-up funds from the University of Maryland School of Medicine (EFM).

Address correspondence to: Jonathan S. Bromberg, University of Maryland School of Medicine, Departments of Surgery and Microbiology and Immunology, 22 South Greene Street, Room S8B06, Baltimore, Maryland 21201, USA. Phone: 410.328.6430; Email: jbromberg@som.umaryland.edu. Or to: Emmanuel F. Mongodin, University of Maryland School of Medicine, Institute for Genome Sciences. Department of Microbiology & Immunology, 801 West Baltimore Street, Room 622, Baltimore, Maryland 21201, USA. Phone: 410.706.6717; Email: emongodin@som.umaryland.edu.

1. Gago M, Cornell LD, Kremers WK, Stegall MD, Cosio FG. Kidney allograft inflammation and fibrosis, causes and consequences. *Am J Transplant*. 2012;12(5):1199–1207.
2. Israni AK, et al. Inflammation in the setting of chronic allograft dysfunction post-kidney transplant: phenotype and genotype. *Clin Transplant*. 2013;27(3):348–358.
3. Moreso F, et al. Immunephenotype of glomerular and interstitial infiltrating cells in protocol renal allograft biopsies and histological diagnosis. *Am J Transplant*. 2007;7(12):2739–2747.
4. Lamb KE, Lodhi S, Meier-Kriesche HU. Long-term renal allograft survival in the United States: a critical reappraisal. *Am J Transplant*. 2011;11(3):450–462.

5. Sellarés J, et al. Inflammation lesions in kidney transplant biopsies: association with survival is due to the underlying diseases. *Am J Transplant*. 2011;11(3):489–499.
6. Koren O, et al. Human oral, gut, and plaque microbiota in patients with atherosclerosis. *Proc Natl Acad Sci USA*. 2011;108 Suppl 1:4592–4598.
7. Wang D, et al. Gut microbiota metabolism of anthocyanin promotes reverse cholesterol transport in mice via repressing miRNA-10b. *Circ Res*. 2012;111(8):967–981.
8. Atkinson MA, Chervonsky A. Does the gut microbiota have a role in type 1 diabetes? Early evidence from humans and animal models of the disease. *Diabetologia*. 2012;55(11):2868–2877.
9. Sonnenberg GF, et al. Innate lymphoid cells promote anatomical containment of lymphoid-resident commensal bacteria. *Science*. 2012;336(6086):1321–1325.
10. Abt MC, et al. Commensal bacteria calibrate the activation threshold of innate antiviral immunity. *Immunity*. 2012;37(1):158–170.
11. Chung H, et al. Gut immune maturation depends on colonization with a host-specific microbiota. *Cell*. 2012;149(7):1578–1593.
12. Josefowicz SZ, et al. Extrathymically generated regulatory T cells control mucosal TH2 inflammation. *Nature*. 2012;482(7385):395–399.
13. Atarashi K, et al. Induction of colonic regulatory T cells by indigenous Clostridium species. *Science*. 2011;331(6015):337–341.
14. Geuking MB, et al. Intestinal bacterial colonization induces mutualistic regulatory T cell responses. *Immunity*. 2011;34(5):794–806.
15. Hooper LV, Littman DR, Macpherson AJ. Interactions between the microbiota and the immune system. *Science*. 2012;336(6086):1268–1273.
16. Lei YM, et al. The composition of the microbiota modulates allograft rejection. *J Clin Invest*. 2016;126(7):2736–2744.
17. Hossain MS, et al. Flagellin, a TLR5 agonist, reduces graft-versus-host disease in allogeneic hematopoietic stem cell transplantation recipients while enhancing antiviral immunity. *J Immunol*. 2011;187(10):5130–5140.
18. Jenq RR, et al. Regulation of intestinal inflammation by microbiota following allogeneic bone marrow transplantation. *J Exp Med*. 2012;209(5):903–911.
19. Dethlefsen L, Relman DA. Incomplete recovery and individualized responses of the human distal gut microbiota to repeated antibiotic perturbation. *Proc Natl Acad Sci USA*. 2011;108 Suppl 1:4554–4561.
20. von Rosenvinge EC, Song Y, White JR, Maddox C, Blanchard T, Fricke WF. Immune status, antibiotic medication and pH are associated with changes in the stomach fluid microbiota. *ISME J*. 2013;7(7):1354–1366.
21. Koren O, et al. Host remodeling of the gut microbiome and metabolic changes during pregnancy. *Cell*. 2012;150(3):470–480.
22. Bhan AK, Mizoguchi E, Smith RN, Mizoguchi A. Colitis in transgenic and knockout animals as models of human inflammatory bowel disease. *Immunol Rev*. 1999;169:195–207.
23. Prinz I, Klemm U, Kaufmann SH, Steinhoff U. Exacerbated colitis associated with elevated levels of activated CD4+ T cells in TCRalpha chain transgenic mice. *Gastroenterology*. 2004;126(1):170–181.
24. Rooks MG, et al. Gut microbiome composition and function in experimental colitis during active disease and treatment-induced remission. *ISME J*. 2014;8(7):1403–1417.
25. Chen X, et al. A mouse model of Clostridium difficile-associated disease. *Gastroenterology*. 2008;135(6):1984–1992.
26. Larsen CP, et al. Long-term acceptance of skin and cardiac allografts after blocking CD40 and CD28 pathways. *Nature*. 1996;381(6581):434–438.
27. Murase N, et al. Heterotopic heart transplantation in the rat receiving FK-506 alone or with cyclosporine. *Transplant Proc*. 1987;19(5 Suppl 6):71–75.
28. Ochiai T, et al. Studies on FK506 in experimental organ transplantation. *Transplant Proc*. 1988;20(1 Suppl 1):209–214.
29. Lennon G, et al. Correlations between colonic crypt mucin chemotype, inflammatory grade and Desulfovibrio species in ulcerative colitis. *Colorectal Dis*. 2014;16(5):O161–O169.
30. Rowan F, Docherty NG, Murphy M, Murphy B, Calvin Coffey J, O'Connell PR. Desulfovibrio bacterial species are increased in ulcerative colitis. *Dis Colon Rectum*. 2010;53(11):1530–1536.
31. Morton AM, Sefik E, Upadhyay R, Weissleder R, Benoist C, Mathis D. Endoscopic photoconversion reveals unexpectedly broad leukocyte trafficking to and from the gut. *Proc Natl Acad Sci USA*. 2014;111(18):6696–6701.
32. Yu H, et al. Intestinal type 1 regulatory T cells migrate to periphery to suppress diabetogenic T cells and prevent diabetes development. *Proc Natl Acad Sci USA*. 2017;114(39):10443–10448.
33. Huang Y, et al. S1P-dependent interorgan trafficking of group 2 innate lymphoid cells supports host defense. *Science*. 2018;359(6371):114–119.
34. Ochando JC, et al. Alloantigen-presenting plasmacytoid dendritic cells mediate tolerance to vascularized grafts. *Nat Immunol*. 2006;7(6):652–662.
35. Ochando JC, et al. Lymph node occupancy is required for the peripheral development of alloantigen-specific Foxp3+ regulatory T cells. *J Immunol*. 2005;174(11):6993–7005.
36. Burrell BE, Bromberg JS. Fates of CD4+ T cells in a tolerant environment depend on timing and place of antigen exposure. *Am J Transplant*. 2012;12(3):576–589.
37. Burrell BE, Warren KJ, Nakayama Y, Iwami D, Brinkman CC, Bromberg JS. Lymph Node Stromal Fiber ER-TR7 Modulates CD4+ T Cell Lymph Node Trafficking and Transplant Tolerance. *Transplantation*. 2015;99(6):1119–1125.
38. Nakayama Y, Brinkman CC, Bromberg JS. Murine Fibroblastic Reticular Cells From Lymph Node Interact With CD4+ T Cells Through CD40-CD40L. *Transplantation*. 2015;99(8):1561–1567.
39. Nakayama Y, Bromberg JS. Lymphotoxin-beta receptor blockade induces inflammation and fibrosis in tolerized cardiac allografts. *Am J Transplant*. 2012;12(9):2322–2334.
40. Dasoveanu DC, Shipman WD, Chia JJ, Chyou S, Lu TT. Regulation of Lymph Node Vascular-Stromal Compartment by Dendritic Cells. *Trends Immunol*. 2016;37(11):764–777.
41. Chyou S, et al. Coordinated regulation of lymph node vascular-stromal growth first by CD11c+ cells and then by T and B cells. *J Immunol*. 2011;187(11):5558–5567.
42. Kumar V, et al. A dendritic-cell-stromal axis maintains immune responses in lymph nodes. *Immunity*. 2015;42(4):719–730.
43. Warren KJ, Iwami D, Harris DG, Bromberg JS, Burrell BE. Laminins affect T cell trafficking and allograft fate. *J Clin Invest*.

2014;124(5):2204–2218.
44. Fonseca DM, et al. Microbiota-Dependent Sequelae of Acute Infection Compromise Tissue-Specific Immunity. *Cell*. 2015;163(2):354–366.
45. Ding Y, Qin L, Kotenko SV, Pestka S, Bromberg JS. A single amino acid determines the immunostimulatory activity of interleukin 10. *J Exp Med*. 2000;191(2):213–224.
46. Falony G, et al. Population-level analysis of gut microbiome variation. *Science*. 2016;352(6285):560–564.
47. Manichanh C, et al. Reshaping the gut microbiome with bacterial transplantation and antibiotic intake. *Genome Res*. 2010;20(10):1411–1419.
48. Zhernakova A, et al. Population-based metagenomics analysis reveals markers for gut microbiome composition and diversity. *Science*. 2016;352(6285):565–569.
49. Schroeder BO, Bäckhed F. Signals from the gut microbiota to distant organs in physiology and disease. *Nat Med*. 2016;22(10):1079–1089.
50. Van Praet JT, et al. Commensal microbiota influence systemic autoimmune responses. *EMBO J*. 2015;34(4):466–474.
51. Simon T, Bromberg JS. Regulation of the Immune System by Laminins. *Trends Immunol*. 2017;38(11):858–871.
52. Shankar J, et al. Looking Beyond Respiratory Cultures: Microbiome-Cytokine Signatures of Bacterial Pneumonia and Tracheobronchitis in Lung Transplant Recipients. *Am J Transplant*. 2016;16(6):1766–1778.
53. Kakihana K, et al. Fecal microbiota transplantation for patients with steroid-resistant acute graft-versus-host disease of the gut. *Blood*. 2016;128(16):2083–2088.
54. Oh PL, Martínez I, Sun Y, Walter J, Peterson DA, Mercer DF. Characterization of the ileal microbiota in rejecting and nonrejecting recipients of small bowel transplants. *Am J Transplant*. 2012;12(3):753–762.
55. Fricke WF, Maddox C, Song Y, Bromberg JS. Human microbiota characterization in the course of renal transplantation. *Am J Transplant*. 2014;14(2):416–427.
56. Dickson RP, et al. Changes in the lung microbiome following lung transplantation include the emergence of two distinct Pseudomonas species with distinct clinical associations. *PLoS ONE*. 2014;9(5):e97214.
57. Lee JR, et al. Gut microbiota and tacrolimus dosing in kidney transplantation. *PLoS One*. 2015;10(3):e0122399.
58. Lee JR, et al. Gut microbial community structure and complications after kidney transplantation: a pilot study. *Transplantation*. 2014;98(7):697–705.
59. Lemahieu W, Maes B, Verbeke K, Rutgeerts P, Geboes K, Vanrenterghem Y. Cytochrome P450 3A4 and P-glycoprotein activity and assimilation of tacrolimus in transplant patients with persistent diarrhea. *Am J Transplant*. 2005;5(6):1383–1391.
60. Willner DL, et al. Reestablishment of recipient-associated microbiota in the lung allograft is linked to reduced risk of bronchiolitis obliterans syndrome. *Am J Respir Crit Care Med*. 2013;187(6):640–647.
61. Fanning S, et al. Bifidobacterial surface-exopolysaccharide facilitates commensal-host interaction through immune modulation and pathogen protection. *Proc Natl Acad Sci USA*. 2012;109(6):2108–2113.
62. Salazar N, et al. Immune modulating capability of two exopolysaccharide-producing Bifidobacterium strains in a Wistar rat model. *Biomed Res Int*. 2014;2014:106290.
63. Schiavi E, et al. The Surface-Associated Exopolysaccharide of Bifidobacterium longum 35624 Plays an Essential Role in Dampening Host Proinflammatory Responses and Repressing Local TH17 Responses. *Appl Environ Microbiol*. 2016;82(24):7185–7196.
64. López P, et al. Interaction of Bifidobacterium bifidum LMG13195 with HT29 cells influences regulatory-T-cell-associated chemokine receptor expression. *Appl Environ Microbiol*. 2012;78(8):2850–2857.
65. Nguyen TL, Vieira-Silva S, Liston A, Raes J. How informative is the mouse for human gut microbiota research? *Dis Model Mech*. 2015;8(1):1–16.
66. Belkaid Y, Hand TW. Role of the microbiota in immunity and inflammation. *Cell*. 2014;157(1):121–141.
67. Hand TW, Vujkovic-Cvijin I, Ridaura VK, Belkaid Y. Linking the Microbiota, Chronic Disease, and the Immune System. *Trends Endocrinol Metab*. 2016;27(12):831–843.
68. van den Elsen LW, Poyntz HC, Weyrich LS, Young W, Forbes-Blom EE. Embracing the gut microbiota: the new frontier for inflammatory and infectious diseases. *Clin Transl Immunology*. 2017;6(1):e125.
69. Khokhlova EV, Smeianov VV, Efimov BA, Kafarskaia LI, Pavlova SI, Shkoporov AN. Anti-inflammatory properties of intestinal Bifidobacterium strains isolated from healthy infants. *Microbiol Immunol*. 2012;56(1):27–39.
70. van Baarlen P, Wells JM, Kleerebezem M. Regulation of intestinal homeostasis and immunity with probiotic lactobacilli. *Trends Immunol*. 2013;34(5):208–215.
71. Villena J, Kitazawa H. Modulation of Intestinal TLR4-Inflammatory Signaling Pathways by Probiotic Microorganisms: Lessons Learned from Lactobacillus jensenii TL2937. *Front Immunol*. 2014;4:512.
72. Ménard O, Gafa V, Kapel N, Rodriguez B, Butel MJ, Waligora-Dupriet AJ. Characterization of immunostimulatory CpG-rich sequences from different Bifidobacterium species. *Appl Environ Microbiol*. 2010;76(9):2846–2855.
73. Turroni F, et al. Characterization of the serpin-encoding gene of Bifidobacterium breve 210B. *Appl Environ Microbiol*. 2010;76(10):3206–3219.
74. Hidalgo-Cantabrana C, Sánchez B, Milani C, Ventura M, Margolles A, Ruas-Madiedo P. Genomic overview and biological functions of exopolysaccharide biosynthesis in Bifidobacterium spp. *Appl Environ Microbiol*. 2014;80(1):9–18.
75. Ferrario C, et al. Modulation of the eps-ome transcription of bifidobacteria through simulation of human intestinal environment. *FEMS Microbiol Ecol*. 2016;92(4):fiw056.
76. Mongodin EF, Hittle LL, Nadendla S, Brinkman CC, Xiong Y, Bromberg JS. Complete Genome Sequence of a Strain of Bifidobacterium pseudolongum Isolated from Mouse Feces and Associated with Improved Organ Transplant Outcome. *Genome Announc*. 2017;5(40):e01089.
77. Grubin CE, Kovats S, deRoos P, Rudensky AY. Deficient positive selection of CD4 T cells in mice displaying altered repertoires of MHC class II-bound self-peptides. *Immunity*. 1997;7(2):197–208.
78. Corry RJ, Winn HJ, Russell PS. Primarily vascularized allografts of hearts in mice. The role of H-2D, H-2K, and non-H-2 antigens in rejection. *Transplantation*. 1973;16(4):343–350.
79. Nagano H, Mitchell RN, Taylor MK, Hasegawa S, Tilney NL, Libby P. Interferon-gamma deficiency prevents coronary

arteriosclerosis but not myocardial rejection in transplanted mouse hearts. *J Clin Invest*. 1997;100(3):550–557.
80. Jackson HT, Mongodin EF, Davenport KP, Fraser CM, Sandler AD, Zeichner SL. Culture-independent evaluation of the appendix and rectum microbiomes in children with and without appendicitis. *PLoS ONE*. 2014;9(4):e95414.
81. Zupancic ML, et al. Analysis of the gut microbiota in the old order Amish and its relation to the metabolic syndrome. *PLoS ONE*. 2012;7(8):e43052.
82. Fadrosh DW, et al. An improved dual-indexing approach for multiplexed 16S rRNA gene sequencing on the Illumina MiSeq platform. *Microbiome*. 2014;2(1):6.
83. Caporaso JG, et al. Ultra-high-throughput microbial community analysis on the Illumina HiSeq and MiSeq platforms. *ISME J*. 2012;6(8):1621–1624.
84. Masella AP, Bartram AK, Truszkowski JM, Brown DG, Neufeld JD. PANDAseq: paired-end assembler for illumina sequences. *BMC Bioinformatics*. 2012;13:31.
85. Caporaso JG, et al. QIIME allows analysis of high-throughput community sequencing data. *Nat Methods*. 2010;7(5):335–336.
86. DeSantis TZ, et al. Greengenes, a chimera-checked 16S rRNA gene database and workbench compatible with ARB. *Appl Environ Microbiol*. 2006;72(7):5069–5072.
87. Paulson JN, Stine OC, Bravo HC, Pop M. Differential abundance analysis for microbial marker-gene surveys. *Nat Methods*. 2013;10(12):1200–1202.
88. Oksanen J, et al. vegan: Community Ecology Package. CRAN R-Project. https://CRAN.R-project.org/package=vegan. Accessed September 7, 2018.
89. McMurdie PJ, Holmes S. phyloseq: an R package for reproducible interactive analysis and graphics of microbiome census data. *PLoS One*. 2013;8(4):e61217.
90. Huber W, et al. Orchestrating high-throughput genomic analysis with Bioconductor. *Nat Methods*. 2015;12(2):115–121.
91. Paulson JN, Olson ND, Wagner J, Talukder H, Pop M, Bravo HC. Statistical analysis for sparse high-throughput sequencing. Bioconductor. https://www.bioconductor.org/packages/release/bioc/manuals/metagenomeSeq/man/metagenomeSeq.pdf. Published July 21, 2016. Accessed September 7, 2018.
92. McMurdie, JP. JNP. biomformat: An interface package for the BIOM file format. https://github.com/joey711/biomformat/, http://biom-format.org.
93. Wickham H. *ggplot2: elegant graphics for data analysis*. New York, New York: Springer-Verlag New York; 2009.
94. Shannon CE. A mathematical theory of communication. *ACM SIGMOBILE Mobile Computing and Communications Review*. 2001;5(1):3–55.
95. Li W, Godzik A. Cd-hit: a fast program for clustering and comparing large sets of protein or nucleotide sequences. *Bioinformatics*. 2006;22(13):1658–1659.
96. Fu L, Niu B, Zhu Z, Wu S, Li W. CD-HIT: accelerated for clustering the next-generation sequencing data. *Bioinformatics*. 2012;28(23):3150–3152.
97. Goetzinger KR, Tuuli MG, Odibo AO. Statistical analysis and interpretation of prenatal diagnostic imaging studies, part 3: approach to study design. *J Ultrasound Med*. 2011;30(10):1415–1423.
98. Segata N, et al. Metagenomic biomarker discovery and explanation. *Genome Biol*. 2011;12(6):R60.
99. Love MI, Huber W, Anders S. Moderated estimation of fold change and dispersion for RNA-seq data with DESeq2. *Genome Biol*. 2014;15(12):550.
100. Weiss SJ, et al. Effects of library size variance, sparsity, and compositionality on the analysis of microbiome data. PeerJ PrePrints. https://peerj.com/preprints/1157/. Published June 3, 2015. Accessed September 7, 2018.